Resonant response of a moonpool with a recess

by J. N. Newman
<jnn@mit.edu>
MIT, Cambridge, MA 02139, USA
WAMIT, Inc., Chestnut Hill, MA 02467, USA
postal address: 1 Bowditch Rd, Woods Hole, MA 02543, USA

April 15, 2018

Abstract

Resonant modes of motion are analyzed in a moonpool with a recess, of the same type studied by Guo et al [1,2] and Molin [3]. The length and depth of the recess are varied, as in [3]. The moonpool is placed within a rectangular barge, which has dimensions similar to the drillship in [1,2]. The complete structure consisting of the barge and moonpool is analyzed by solving the diffraction problem with incident waves, and the resonant frequencies are found which maximize the free-surface elevation in the moonpool. The resonant frequencies are also identified with singularities in the surge and heave added-mass coefficients. These results are compared with different approximations, which may be useful for estimating the resonant frequencies. In the simplest approximation the resonant frequencies of sloshing modes are determined from the wavelengths of standing waves in a closed basin with the same length as the moonpool. More rational and complete approximations are developed similar to those in [3], with the moonpool and exterior fluid domain analyzed separately and the solutions matched at the interface. This leads to a linear system of equations involving generalized added-mass coefficients in the two domains. Analytical and numerical methods are described for the evaluation of these coefficients.

1 Introduction

Moonpools on ships are enclosed volumes of water which are open from the bottom to the free surface, to facilitate drilling and other marine operations. Oscillations in moonpools are induced by the external wave field and by motions or forward speed of the ship. These oscillations are damped by external wave radiation, and also by viscous and nonlinear effects, but in typical configurations the damping is weak. Thus the moonpool oscillations can be resonant, with large amplitudes which disrupt the operations.

The simplest types of moonpools are cylindrical with vertical walls, opening at the bottom to the external fluid domain beneath the hull. Two types of resonant motion exist, known as the piston and sloshing modes. These are described by Faltinsen & Timokha [4]. The piston mode, also known as the pumping or Helmholtz mode, is predominantly vertical. It can be

approximated by considering the fluid in the moonpool to oscillate with uniform motion like a heaving rigid body. Resonance occurs when the inertia force of this quasi-rigid mass is equal to the hydrostatic restoring force, with the resulting resonant frequency $\omega_0 = \sqrt{g/d}$ where g is the gravitational acceleration and d the draft. The sloshing modes are similar to standing waves in a closed tank. For a rectangular moonpool with length ℓ longitudinal sloshing modes occur when ℓ is an integer multiple of a half-wavelength. For waves in deep water the corresponding resonant frequencies are $\omega_n = \sqrt{\pi n g/\ell}$ where $(n = 1, 2, 3, ...)$. The accuracy of these approximations must be confirmed since they ignore interactions between the moonpool and the exterior fluid domain. Their validity is more questionable for moonpools with boundary surfaces which are not completely vertical and cylindrical.

Guo et al [1,2] performed experiments with a model of a ship containing a moonpool with a recess, to study the occurrence of resonance for this configuration. The recess is a longitudinal extension of the upper part of the moonpool including the free surface, as shown in Figures 1 and 2. Molin [3] has developed a method for computing the resonant frequencies, based on an extension of his earlier method [5] for moonpools with vertical walls. In this case a more complicated flow exists between the two parts of the moonpool, and the distinction between the piston and sloshing modes is less clear. In general there is a nonzero flux of fluid in and out of the moonpool for all of the resonant modes. Nevertheless it is useful to distinguish between the piston and sloshing modes. Thus the resonant mode with the lowest frequency is defined as the piston mode and the others are defined as sloshing modes, ordered in accordance with their frequencies.

The present study expands on the work in [3], focusing on the evaluation of the natural frequencies for a moonpool with a recess using several different approaches. In Section 2 a direct global approach is followed using the radiation-diffraction code WAMIT to analyze the rectangular barge shown in Figure 2. This vessel has dimensions similar to the drillship in [1,2]. Computations of the free-surface elevation in the moonpool are made with the vessel fixed in head waves. The frequencies where the moonpool elevation is maximized are defined as resonant. An alternative procedure is discussed where the resonant frequencies are identified by singularities in the surge and heave added-mass coefficients of the vessel. (Here 'singularity' is used somewhat loosely, to refer to numerical results which are bounded but with very large values and rapid variation.) In Section 3 a simple semi-empirical method is described to approximate the sloshing frequencies, based on the wavelength of standing waves in the moonpool.

In Section 4 a more refined approximation is derived based on domain decomposition, with separate solutions in the moonpool and exterior domain. This is similar to the method of Molin [3,5] but a different set of orthogonal functions based on Legendre polynomials is used to represent the normal velocity at the interface between the moonpool and exterior domain. Matching the two solutions at the interface leads to a linear system of equations involving the added-mass coefficients of the interface modes. The resonant frequencies are identified by the zeros of the determinant of these coefficients. Good agreement with the results in Section 2 is achieved with a small number of interface modes. The evaluation of the added-mass coefficients in the moonpool is described in Section 5. Section 6 contains a more complete analysis of the added-mass coefficients in the exterior domain, which shows that the small errors observed in Section 4 are due to the neglect of the exterior free surface and hull shape. Section 7 includes a discussion of the results and conclusions regarding the utility of the approximations. Computational details are described in Appendix A and further details regarding the analytical solutions are included in Appendices B-D.

The analytical and numerical methods are based on the usual assumptions of linearized wave-body interactions, neglecting nonlinear and viscous effects. The same moonpool configuration is used as in [1,2] and [3], with the results presented in full-scale dimensional units of measurement to facilitate comparisons. In addition to the 'base' moonpool configuration of Guo et al [1,2] the variants included in [3] are also considered, where the length or depth of the recess is varied.

2 Global analysis of the vessel

As a direct approach, and basis for comparison with approximations of the resonant frequencies, computations have been made of the diffraction and radiation problems for the vessel shown in Figure 2. This is a simple rectangular barge with dimensions similar to the drillship studied by Guo et al [1,2] and with the same moonpool. The opening at the bottom of the moonpool is centered at the midship section of the barge. The recess is at the aft end of the moonpool.

In the diffraction problem the barge is fixed in head waves. Thus there is no influence from the vessel's motions. Computations are made of the free-surface elevation along the centerline of the moonpool to find the point where the elevation is a maximum. The maximum elevation is shown by the solid line in Figure 3 for the base configuration, as a function of the frequency of the incident waves. The resonant peaks are at $\omega = 0.416$, 0.802, 1.075, 1.338 radians/second. The dashed line in Figure 3 is the mean value of the elevation, which is equal to the volume flux per unit area of the free surface. It is evident that there is substantial volume flux not only for the piston mode, but also for the sloshing modes.

These results can be compared with the experimental results in [1], replotted in Figure 4 of [3]. The most obvious difference is that the computed peaks in Figure 3 are much larger, due to the neglect of nonlinear and viscous effects. It is possible that the experimental peaks are restricted by the spacing of the frequencies shown in Figures 11-13 of [1], but it is obvious that the large computed peaks in Figure 3 are non-physical. The magnitude of the peaks is discussed more extensively in [2], including results from CFD calculations where nonlinear and viscous effects are included. Another difference is with respect to the bandwidth of the resonant peaks; in the experimental results the bandwidth of the piston mode is relatively narrow compared to the first sloshing mode, but the computations in Figure 3 show the opposite comparison. Despite these differences, the positions of the peaks are in good agreement. The only difference which is measurable from the plot in [3] is for the first sloshing frequency, $\omega = 0.802$, where the experimental value is about 0.82.

The point of maximum elevation is at the shallow end of the recess for the piston mode and at the deep end of the moonpool for the first two sloshing modes. These results are substantially consistent with the experimental observations in [1], and with the modal shapes in [3].

Figure 4 shows the magnitudes of the resonant peaks for varying lengths of the recess. The amplitude of the piston mode increases rapidly with increased length; conversely the first sloshing mode is dominant for the cylindrical case, where there is no recess, but it decreases rapidly with increased length of the recess. The amplitudes of the higher sloshing modes are irregular; it is unclear if this is due to reflections and interference, associated with the relatively short wavelengths, or to the numerical difficulty associated with their narrow bandwidths. In view of the narrow bandwidths shown in Figure 3 these higher modes are of less significance from the practical standpoint.

An alternative procedure for evaluating the resonant frequencies is to calculate the added-mass coefficients of the barge, which have singularities at the same frequencies. This is a simpler method since it does not require special calculations or post-processing, but it does not provide information about the magnitude of the free-surface elevation or mode shapes in the moonpool. The added-mass coefficients are shown in Figure 5 for surge and heave motions with no recess (a), and with the base recess (b). The barge with no recess is symmetrical about $x = 0$, and the piston mode and second sloshing mode are symmetrical while the first and third sloshing modes are anti-symmetrical. Thus the piston mode is only indicated by its effect on the heave added mass, which is relatively small due to the vertical sides of the moonpool. The first and third sloshing modes are clearly indicated by their strong effect on the surge added mass. The second sloshing mode affects the heave added mass but only in a very narrow bandwidth; detecting this singularity requires computations at frequency increments of 0.0001. This illustrates the limitations of the procedure for symmetrical or nearly symmetrical vessels. For cases where there is a substantial recess, such as the base configuration in Figure 5(b), the resonant frequencies are clearly indicated by the singularities in both added-mass coefficients. The frequencies where the singularities occur in Figure 5 are practically identical to those where the free-surface elevation in the moonpool is a maximum.

The resonant frequencies for the piston mode and first three sloshing modes are shown by the solid lines in Figures 6 and 8 for varying lengths and depths of the recess. These results are evaluated from the diffraction analysis, based on the maximum amplitudes of the free-surface elevation in the moonpool. The resonant frequencies for all of these modes decrease as the length of the recess increases, or as the depth decreases. No results are shown for depths less than 0.5m since strong nonlinear effects are expected in this regime. Nevertheless it is interesting to note that the results for small depths are completely different from those for small recess lengths, since the fluid domain in the moonpool is the same in both limits. Thus the fluid motion in the shallow region is important even as the depth tends to zero, as in other problems with similar geometry (cf. [6]).

3 Standing-wave approximations

A simple approximation for the frequencies of the sloshing modes can be based on the assumption that the length ℓ of the moonpool is an integer multiple of a half-wavelength. For standing waves in deep water with wavelength λ and wavenumber $K = 2\pi/\lambda$ the frequency is $\omega = \sqrt{gK} = \sqrt{2\pi g/\lambda}$, where g is the gravitational acceleration. These waves will satisfy the boundary condition of zero horizontal velocity at the vertical ends if ℓ is an integer multiple of $\lambda/2$. On this basis the resonant frequencies are

$$\omega_n = \sqrt{\pi n g/\ell} = \sqrt{g k_n}, \tag{1}$$

where $(n = 1, 2, 3, ...)$ and $k_n = \pi n/\ell$. It is logical to use these relations in the deep section of the moonpool where it is open at the bottom, assuming the exterior domain is relatively deep.

In the recess, of constant depth c, it is more appropriate to use the dispersion relation

$$\omega = \sqrt{gk \tanh kc}. \tag{2}$$

Thus, for the same values of $k = k_n$, the frequency is reduced. This implies that (1) will over-predict the resonant frequencies for a moonpool with a recess, as shown for the second and third sloshing modes by the short dashed lines in Figure 6.

As a pragmatic approximation the weighted average of the frequencies is defined, based on (1) in the deep part of the moonpool of length $2a$, and (2) in the recess of length b. On this basis

$$\omega_n = \left(2a\sqrt{gk_n} + b\sqrt{gk_n \tanh k_n c}\right) \Big/ (2a+b) \tag{3}$$

where $k_n = \pi n/(2a+b)$. The results of this approximation are shown by the longer dashed lines in Figure 6. The accuracy is improved considerably for the second and third sloshing modes. For the first sloshing mode the accuracy is in fact better using (1), except for the smallest lengths and depths of the recess; this may be due to a fortuitous cancellation of effects which are not included in the approximation.

4 Domain decomposition

The coupling between the motions in the moonpool and external fluid can be analyzed by considering these domains separately, with a common interfacial boundary in the horizontal plane at the bottom of the moonpool. This approach has been developed by Molin [3,5], and by Faltinsen & Timokha [4]. Continuity at the interface is achieved by expanding the normal velocity in a set of Fourier functions and using the Galerkin method to derive a linear system of equations for the coefficients of the expansion. The resonant frequencies in the moonpool follow as the eigenfrequencies of this linear system. In [3] the expansions are truncated after 10 or 20 terms, which implies a substantial computational effort to set up and solve the linear systems.

One advantage of this approach is that different simplifying assumptions can be used which are appropriate in each domain. Most importantly, it is assumed that the external domain is bounded above by an infinite horizontal plane with a homogeneous Neumann boundary condition (zero vertical velocity) applied everywhere outside the opening of the moonpool.

A similar approach is followed here, with the same assumptions as in [3], but Legendre polynomials are used instead of Fourier functions. Both sets of functions have been compared in preliminary computations, and the convergence at the second and third sloshing modes is improved slightly with polynomials. The use of polynomials also permits the external added-mass coefficients to be represented by integrals which can be evaluated analytically for all modes of the interface, as shown in Appendix B.

The motion is assumed to be monochromatic, with frequency ω. Following the notation in [3] the velocity potentials in the moonpool and external domain are denoted by ϕ^+ and ϕ^-, respectively. Both potentials satisfy the Laplace equation in their respective domains. The potential ϕ^+ satisfies the free-surface condition

$$K\phi^+ - \phi^+_z = 0 \qquad \text{on } z = 0, \tag{4}$$

where $K = \omega^2/g$. The homogeneous Neumann condition $\phi^+_n = 0$ is satisfied on the sides and ends of the moonpool and bottom of the recess. In the external domain the boundary condition $\phi^-_z = 0$ is satisfied on $z = -d$ outside the moonpool opening, and ϕ^- is assumed to vanish at infinity.

On the interface boundary shown by the dashed line in Figure 1 the potential and its normal derivative are continuous. Thus

$$\phi^+ = \phi^- \tag{5}$$

and

$$\phi_z^+ = \phi_z^- = \mathrm{i}\omega f(x,y), \tag{6}$$

where $f(x,y)$ is the vertical deflection of the interface. If the moonpool is relatively narrow, and only longitudinal resonant modes are considered, the deflection is independent of y and can be expanded in the form

$$f(x) = \sum_{i=1}^{\infty} c_i f_i(x), \ -a < x < a, \tag{7}$$

where $f_i(x)$ is a suitable set of basis functions in the interval $(-a, a)$.

The velocity potentials are expanded in a similar form, with

$$\phi^{\pm} = \mathrm{i}\omega \sum_{i=1}^{\infty} c_i \phi_i^{\pm}, \tag{8}$$

where

$$\phi_{iz}^{\pm} = f_i(x) \qquad \text{on } z = -d, \ -a < x < a. \tag{9}$$

Each of the basis functions $f_i(x)$ defines a mode of vertical motion at the interface. Where confusion is possible these are referred to as 'interface modes', to distinguish them from the piston and sloshing modes of the free surface.

As in conventional radiation problems for rigid-body motions, generalized added-mass coefficients can be defined for the interface modes as

$$A_{ij}^{\pm} = \iint_{\mathcal{B}} \phi_i^{\pm} \phi_{jn}^{\pm} dS = \mp \iint_{\mathcal{B}} \phi_i^{\pm} \phi_{jz}^{\pm} dS, \tag{10}$$

where $\mathcal{B}$ denotes the interface at the bottom of the moonpool, and the normal vector is directed out of each domain. For convenience the fluid density ρ is omitted, since it does not affect the use of the added-mass coefficients for matching the potential and normal velocity. There is no damping due to wave radiation in the closed domain of the moonpool, or in the external domain where the upper boundary is rigid.

Using the Galerkin method to satisfy the matching condition (5),

$$\iint_{\mathcal{B}} f_j(x) \left(\phi^+(x) - \phi^-(x)\right) dx = \mathrm{i}\omega \sum_{i=1}^{\infty} c_i \iint_{\mathcal{B}} f_j(x) \left(\phi_i^+(x) - \phi_i^-(x)\right) dx = 0, \tag{11}$$

for all values of j. After substituting (9) and (10),

$$\sum_{i=1}^{\infty} c_i \left(A_{ij}^+ + A_{ij}^-\right) = 0. \tag{12}$$

Thus the matching condition is reduced to the solution of a linear system involving the added-mass coefficients for the two domains. Eigensolutions which represent the resonant modes of the moonpool will exist if and only if the determinant of this system is zero:

$$\left|A_{ij}^+ + A_{ij}^-\right| = 0. \tag{13}$$

Hereafter the infinite system is truncated, at order $i = N$, and calculations are made using Legendre polynomials with $N = 1, 2, 3, 4$. Thus

$$f(x) = \sum_{i=1}^{N} c_i P_{i-1}(x'), \tag{14}$$

where $x' = x/a$ is in the interval $(-1, 1)$ and P_{i-1} is the Legendre polynomial of degree $(i-1)$. The first four of these orthogonal functions are

$$P_0(x') = 1,\ P_1(x') = x',\ P_2(x') = \tfrac{3}{2}x'^2 - \tfrac{1}{2},\ P_3(x') = \tfrac{5}{2}x'^3 - \tfrac{3}{2}x'.$$

The first interface mode is a uniform deflection with unit amplitude, analogous to heave, with nonzero volume flux; the second is an angular rotation about the center of the opening, analogous to pitch, with unit amplitude at $x = \pm a$.

Figure 7 shows the determinant (13) for the base moonpool with the truncation order $N = 1, 2, 3, 4$. The first two zero-crossings are near $\omega = 0.40$ and $\omega = 0.77$, where all four curves vary smoothly, indicating the piston mode and first sloshing mode. At the intermediate point near $\omega = 0.53$ there is a singularity, due to the existence of a homogeneous solution which corresponds to the first sloshing mode of a tank with the same geometrical configuration and a fixed bottom. The second sloshing mode of the moonpool is indicated by the zero-crossings for $N = 2, 3, 4$ near $\omega = 1.07$. At higher frequencies it is not possible to identify the zero-crossings clearly from the plot; careful examination of the numerical data is necessary to distinguish the zero-crossing at the third sloshing frequency from the adjacent singularity.

Figure 8 compares the resonant frequencies obtained from this method with the results from the diffraction analysis, for the same lengths and depths of the recess as in Figure 6. $N = 1$ is sufficient to provide a useful approximation for the piston mode. The maximum errors are a frequency difference of .04 rad/sec for the case where the recess length is zero, and .07 rad/sec when the recess depth is 11m. In the latter case the $N = 2$ approximation is somewhat better. For the first sloshing mode $N = 2$ is necessary for small values of the recess length since this mode is antisymmetric about the center if there is no recess, but for recess lengths greater than 5-10m the approximation using $N = 1$ is surprisingly good. The approximation with $N = 2$ is good for all cases. Similarly, for the second sloshing mode, the $N = 2$ approximation is good for recess lengths greater than 2m, and the $N = 3$ approximation is good in all cases. For the third sloshing mode the results using $N = 4$ give good approximations for all cases and $N = 3$ is good for recess lengths greater than 2m.

For the piston mode and first sloshing mode the results shown in Figure 8 with $N = 2$ appear to be identical to Molin's results shown in Figures 8 and 12 of [3].

If $N = 1$ the resonance condition (13) is simply

$$A_{11}^{+} + A_{11}^{-} = 0. \tag{15}$$

In the exterior domain the added mass A_{11}^{-} is positive, but in the moonpool A_{11}^{+} is negative for some frequencies, as shown in Section 5 and Figure 9(a). It is notable that approximations for both the piston mode and first sloshing mode can be obtained from (15), with only one interface mode of uniform vertical motion, if the errors shown in Figure 8 are acceptable.

The method of domain decomposition used here is fundamentally valid, if a sufficient number of interface modes are included to give converged results and accurate matching of the two solutions. The only approximations are to simplify the separate solutions in the two domains. In the moonpool two-dimensional motion is assumed implicitly, by using only longitudinal mode shapes for matching. This is logical if the moonpool is relatively narrow compared to its length, and if the dominant modes of resonant motion are longitudinal. In the external domain it has been assumed that free-surface effects are not important, and that the upper boundary is an infinite rigid horizontal plane outside the opening of the moonpool. These assumptions

are examined in Section 6, where it will be shown that they account for the small differences observed in Figure 8.

5 Analytical evaluation of the moonpool added mass

Following [3], the velocity potential in the moonpool can be evaluated analytically using two rectangular domains, separated by an interface at $z = -c$. Here the velocity potential is denoted by φ^+ in the upper domain and by φ^- in the lower domain. Two-dimensional motion is assumed. Our attention is restricted to the added-mass coefficients A^+_{11} and A^+_{22}, defined by (10), and the cross-coupling coefficients $A^+_{12} = A^+_{21}$. The only solutions required are where φ^- satisfies the boundary condition (9) with $f_1(x) = 1$ and $f_2(x) = x/a$. The corresponding potentials in the two domains are denoted by $\varphi^\pm_1$ and $\varphi^\pm_2$.

The general solutions in the upper domain satisfy the free-surface condition (4) and homogeneous Neumann conditions on the vertical walls at $x = -a$ and $x = a + b$. Thus

$$\varphi^+_i = C^{(i)}_0(1 + Kz) + \sum_{m=1}^{\infty} C^{(i)}_m \cos\kappa_m(x + a)\left(\frac{\kappa_m \cosh\kappa_m z + K \sinh\kappa_m z}{\kappa_m \cosh\kappa_m c}\right), \tag{16}$$

where $\kappa_m = m\pi/(2a + b)$ and $K = \omega^2/g$.

The corresponding solutions in the lower domain are

$$\varphi^-_1 \;=\; z + c^{(1)}_0 + \sum_{m=1}^{\infty} c^{(1)}_m \cos k_m(x + a)\left(\frac{\cosh k_m(z + d)}{\cosh k_m(d - c)}\right), \tag{17}$$

$$\begin{aligned}\varphi^-_2 \;=\; & c^{(2)}_0 + \sum_{m=1}^{\infty} c^{(2)}_m \cos k_m(x + a)\left(\frac{\cosh k_m(z + d)}{\cosh k_m(d - c)}\right) \\ & + \sum_{m\ \text{odd}}^{\infty} d^{(2)}_m \cos k_m(x + a)\left(\frac{\cosh k_m(z + c)}{\cosh k_m(d - c)}\right),\end{aligned} \tag{18}$$

where $k_m = m\pi/(2a)$. For odd values of m

$$d^{(2)}_m = \frac{2}{a^2 k^3_m \tanh k_m(d - c)} \tag{19}$$

and for m even $d^{(2)}_m = 0$.

The infinite series in (17) and first series in (18) satisfy $\varphi^-_{iz} = 0$ on $z = -d$. The first term on the right-hand side in (17) represents a uniform vertical motion of the fluid with unit velocity, to satisfy the boundary condition $\varphi^-_{1z} = 1$ on $z = -d$. The second sum in (18) satisfies $\varphi^-_{2z} = x/a$ on $z = -d$ and $\varphi^-_{2z} = 0$ on $z = -c$.

Linear systems of equations can be derived for the unknown coefficients $C^{(i)}_m$ and $c^{(i)}_m$ following a similar procedure as in [3]. The potentials and normal velocities are matched on the interface $z = -c$ and the boundary condition $\varphi^+_{iz} = 0$ is applied on the bottom of the recess. The details are outlined in Appendix C, with the results

$$\sum_{m=0}^{L-1} A_{nm} c^{(i)}_m = B^{(i)}_n \quad (i = 1, 2;\ n = 0, 1, 2, ..., L - 1)\,. \tag{20}$$

Here L is the order of the linear system and

$$A_{00} = a(2a+b), \tag{21}$$

$$A_{nm} = \delta_{mn} a(a+\tfrac{1}{2}b) - k_m \tanh k_m(d-c) \sum_{\mu=1}^{L-1} I_{\mu n} I_{\mu m} \left(\frac{1-(K/\kappa_\mu)\tanh \kappa_\mu c}{K - \kappa_\mu \tanh \kappa_\mu c} \right) \ (m>0), \tag{22}$$

$$B_n^{(1)} = \delta_{0n} a\,(2a/K + bc) + \sum_{\mu=1}^{L-1} I_{\mu n} I_{\mu 0} \left(\frac{1-(K/\kappa_\mu)\tanh \kappa_\mu c}{K - \kappa_\mu \tanh \kappa_\mu c} \right), \tag{23}$$

$$B_n^{(2)} = -\frac{2a+b}{a k_n^3 \sinh k_n(d-c)} \quad (n = 1,3,5,...)\,. \tag{24}$$

In (22) and (23) δ_{mn} is the Kroenecker delta function, equal to 1 if $m=n$ and zero if $m \neq n$. $A_{n0} = 0$ for $n > 0$, and $B_n^{(2)} = 0$ for $n = 0$ or an even integer. The coefficients in (22) and (23) are

$$\begin{aligned} I_{mn} &= (-1)^n \frac{\kappa_m \sin 2a\kappa_m}{\kappa_m^2 - k_n^2} \quad (\kappa_m \neq k_n) \\ &= a \qquad\qquad\qquad\qquad (\kappa_m = k_n)\,. \end{aligned}$$

After solving the linear systems for the unknowns $c_m^{(i)}$ the added-mass coefficients for the moonpool domain can be evaluated from (10). Thus, with w the width,

$$A_{11}^+ = -w \int_{-a}^{a} \varphi_1^-(x,-d)dx = -2aw \left(c_0^{(1)} - d \right), \tag{25}$$

$$A_{22}^+ = -w \int_{-a}^{a} \frac{x}{a} \varphi_2^-(x,-d)dx = \frac{2w}{a} \sum_{m \ \mathrm{odd}} \frac{1}{k_m^2} \left(\frac{c_m^{(2)}}{\cosh k_m(d-c)} + d_m^{(2)} \right). \tag{26}$$

$$A_{12}^+ = -w \int_{-a}^{a} \frac{x}{a} \varphi_1^-(x,-d)dx = \frac{2w}{a} \sum_{m \ \mathrm{odd}} \frac{1}{k_m^2} \left(\frac{c_m^{(1)}}{\cosh k_m(d-c)} \right), \tag{27}$$

$$A_{21}^+ = -w \int_{-a}^{a} \varphi_2^-(x,-d)dx = -2aw c_0^{(2)}. \tag{28}$$

Since $A_{21}^+ = A_{12}^+$ these coefficients can be evaluated from either of the last two equations.

Figure 9 shows the results for the base moonpool configuration, with recess length 16m and depth 3.8m. The linear system is truncated at order $L = 2, 3, 4$. The computations of the same coefficients from WAMIT are also shown for comparison. Near $\omega \simeq 0.4$ the curve for A_{11}^+ using $L = 2$ is shifted so that the approximation of the piston mode frequency using $N = 1$ in Figure 8 would be increased by about 0.04. The results using $L = 3$ or 4 are practically the same as the WAMIT computation. For the first sloshing mode, near $\omega \simeq 0.8$, A_{11}^+ is approximated very well even with $L = 2$, but $L = 3$ or 4 is necessary if the coefficients (26-28) are required.

The 'frozen restriction approximation' described in [3] is equivalent to using only the first two terms on the right-hand side of (17), with a single mode of uniform vertical velocity in the lower domain and on the interface of the upper domain. This causes a singularity at $\omega \simeq 0.416$ where a homogeneous solution exists in the upper domain, as in a rectangular tank with depth c and length $2a+b$. Since the frequency of the piston mode in the base moonpool is almost the same it is not feasible to use this approximation directly. In [3] this problem is avoided by using the zero-frequency limit of the modified added-mass, shown by the short curve in the upper-left corner of Figure 9(a). This under-estimates the added mass for $\omega > 0$, and thus over-estimates the resonant frequency where (15) is satisfied. This may explain the observation in [3] that the frozen restriction approximation over-estimates the resonant frequency of the piston mode.

Using $L \geq 2$ avoids the singularity associated with the homogeneous solution in the upper domain, by including additional modes of vertical velocity which can be balanced to give a bounded solution of the linear system. However the matrix $[\mathbf{A}]$ in (20) may be ill-conditioned in the vicinity of the singular frequency $\omega \simeq 0.416$, and this will affect the solution in a very narrow band of frequencies. This is not evident in Figure 9, where the computations are performed using double precision with the closest computational points at $\omega = 0.41$ and 0.42.

For small values of the frequency ω and wavenumber K the right-hand side of the linear system (20) is dominated by the first term in (23). It follows that

$$c_0^{(1)} \simeq \frac{2a}{K(2a+b)}, \tag{29}$$

and thus, from (25), that

$$A_{11}^{+} \simeq -\frac{4a^2 w}{K(2a+b)}. \tag{30}$$

This result has been derived by Molin [3, Appendix A] using the frozen restriction approximation. An alternative derivation of (30) which is applicable to moonpools of arbitrary shape is given in Appendix D. The asymptotic behavior of (30) for low frequencies is evident in Figure 9(a); the modified coefficients in the upper left corner of this figure are included to show how the remaining non-singular part of A_{11}^{+} varies with the frequency.

6 Added mass in the external domain

An important simplification in the method described in Section 4 is to neglect free-surface effects in the external domain, and to assume that the upper boundary of this domain is an infinite horizontal plane with zero normal velocity outside the opening of the moonpool. These assumptions can be justified if the ship's bottom is flat and the horizontal dimensions are large, but for typical ships the beam is not substantially larger than the dimensions of the moonpool opening. Nevertheless the results in Figure 8 show that these assumptions lead to useful approximations for the resonant frequencies.

A more complete analysis of the external domain can be made, without the assumptions of Section 4, to provide a better understanding of their validity. For this purpose the barge shown in Figure 2 is considered as in Section 2, but the moonpool is replaced by a rectangular patch on the bottom which replaces the opening. On this patch the same modes of normal velocity are specified as are used on the interface in Section 4. The added mass (and damping) are computed for these modes in the external domain, including the effects of the free surface and the three-dimensional shape of the barge.

Figure 10 shows the added-mass coefficients A_{11}^{-} and A_{22}^{-}. Also shown for comparison are the corresponding results described in Section 4 with the assumption of a rigid infinite horizontal plane outside the moonpool, and the results for a barge of zero draft ($d = 0$) with the same waterplane. The later results, shown by the dash-dot lines in Figure 10, are included to show separately the effects of the two assumptions (a) replacing the hull surface by a flat plane in the free surface, and (b) imposing the boundary condition of zero normal velocity on the free surface, which is equivalent to evaluating the added mass at zero frequency. The results show that the assumptions in Section 4 over-estimate A_{11}^{-} slightly at low frequencies, increasing to about 10% in the vicinity of the piston mode and 20% at the first sloshing mode. Most of this

over-estimate is due to the neglect of free-surface effects, but the dash-dot curve for a barge of zero draft on the free surface also over-estimates A_{11}^- for most frequencies, by a smaller amount. For A_{22}^- the three results in Figure 10 are practically identical, with a maximum difference of about 1%.

Since the mode $i = 1$ has nonzero volume flux, the potential decays relatively slowly like a source in the far field. Thus it is not surprising that free-surface effects and the three-dimensional shape of the hull are significant for this mode. Neglecting these effects is more appropriate for the second mode since there is no net flux and the potential is dipole-like with more rapid attenuation in the far field.

Over-estimating A_{11}^- increases the determinants in Figure 7 and moves their zero-crossings to the left. Thus with the approximations in Section 4 the resonant frequencies are under-predicted by a small amount for the piston mode and by a larger amount for the first sloshing mode. This explains the results for these modes shown by the dashed lines in Figure 8.

Figure 10 also shows the normalized damping coefficient B_{11}^-/ω for mode 1, which is much smaller than the added mass. The coefficient B_{22}^-/ω is not shown since its maximum value is less than 1% of A_{22}^-.

7 Discussion and Conclusions

Wave-induced motions are analyzed for a moonpool with a recess of the type considered by Guo et al [1,2] and Molin [3]. Attention is focused on the resonant modes of fluid motion in the moonpool, and the frequencies where these occur.

A direct diffraction analysis is described in Section 2 for a rectangular barge with similar dimensions to the drillship in [1,2]. The radiation-diffraction code WAMIT is used to compute the free-surface elevation in the moonpool and to find the frequencies where this is maximized. The resonant amplitudes are unrealistically large, due to the neglect of viscous and nonlinear effects, but the frequencies where they occur agree well with the experimental results in [1] and with the theoretical estimates in [3]. An alternative procedure is also described in Section 2, based on computations of the vessel's surge and heave added-mass coefficients, which are singular at the resonant frequencies of the moonpool. This procedure is simpler, but it does not provide information about the magnitude or shape of the resonant modes and it can fail to identify some modes if the recess length is small or zero.

In Section 3 a simple method is proposed to estimate the resonant sloshing frequencies, based on a semi-empirical approximation of the wavelength of standing waves in the moonpool. Comparison with the results in Section 2 shows that this method is useful for qualitative purposes, especially with the second and third sloshing modes where the wavelength is relatively short and the effects of the exterior flow outside the moonpool are less important.

The approach described in Section 4, which is similar to the method developed by Molin [3,5], is more rational and complete. The domains of the moonpool and external flow are analyzed separately, with matching of the solutions at the interface in the opening of the moonpool at the bottom of the ship. Legendre polynomials are used to represent the vertical velocity at the interface. The first two modes correspond to displacements of the interface similar to heave and pitch. The amplitudes of the interfacial modes are given by the solution of a linear system of equations involving the added-mass coefficients for the two domains. The order of this linear

system is the same as the number of interfacial modes retained. The resonant frequencies are determined as the frequencies where the determinant of the coefficient matrix for the linear system is zero. Good approximations are demonstrated for the piston mode and first sloshing mode in the moonpool using only the heave and pitch interface modes, and for the second and third sloshing modes using one or two additional interface modes.

The added-mass coefficients used for the results in Sections 4-6 for both the moonpool and exterior domain have been computed using WAMIT, as described in Appendix A. Analytical methods to compute the same added-mass coefficients are described in Section 5 and Appendices B-D; these permit the method in Section 4 to be implemented without using a general radiation-diffraction code.

It is assumed in Section 4 that the motion in the entire exterior domain outside the moonpool is bounded above by an infinite rigid plane at the same depth as the bottom of the ship. Section 6 describes a more complete solution for the exterior domain which includes free-surface effects and the three-dimensional hull shape. The interface with the moonpool is replaced by a patch on the bottom, where generalized modes of motion are defined with the same vertical velocities as in the matching procedure of Section 4. The added-mass coefficients are evaluated for the first two modes, and compared with the results in Section 4. This shows that the added mass of the first interface mode is over-predicted by the assumptions in Section 4, and the frequencies of the piston mode and first sloshing mode are under-predicted.

In the analysis of the moonpool elevation in Section 2, and also in the approach based on domain decomposition in Section 4, the surge, heave and pitch motions of the barge are not included. Additional computations have been made to investigate the influence of these motions on the resonant frequencies using the global analysis described in Section 2, with the barge free to respond to the incident waves. Both the base configuration and the moonpool with no recess have been used for these computations. The changes in the resonant frequencies are small or non-existent. The largest changes are an increase for the piston-mode frequency from 0.749 to 0.769 for the moonpool with no recess, and for the first sloshing mode from 0.802 to 0.824 for the base configuration. Thus the effect of the rigid-body motions on the resonant frequencies is very small, at least for these configurations. This is consistent with the observation noted in Section 2, and also by Molin [3], that the estimates of the resonant frequencies based on fixed body motions are in good agreement with the experiments of Guo et al [1], where the model was free to respond to the incident waves. This differs from the conclusion of Fredriksen et al [7], who found from two-dimensional computations and experiments that the piston-mode period was reduced from 0.88 sec when the body is fixed to coincide with the natural period of heave at 0.75 sec when it is free. It is likely that the interaction between heave and the piston mode is exaggerated in the two-dimensional case, which is similar to the barge with a moonpool that extends throughout the entire length of the hull.

To summarize the results for practical purposes, it is evident that the resonant frequencies of the piston mode and first sloshing mode can be estimated using either a global analysis as in Section 2, or by using the method described in Section 4 with only two interfacial modes (similar to heave and pitch). The frequencies of the higher-order sloshing modes can be approximated with the simple semi-empirical analysis described in Section 3; the comparison in Figure 6 suggests that the first sloshing mode can also be approximated using the simple infinite-depth estimate (1), for recess depths greater than 3m, but the lack of a rational explanation for this agreement implies that it should be used with caution.

Appendix A – Computational details

The computations described in Section 2 have been performed using the radiation-diffraction code WAMIT [8]. The surface of the barge and moonpool is represented by flat quadrilateral patches as shown in Figure 2. The higher-order option is used, with the solution for the velocity potential represented on each patch by continuous B-splines. For the case where the depth in the recess is equal to the draft (11m), a dipole patch is used to represent the surface of zero thickness at the bottom of the recess, as explained in [8], Section 7.10. Field points on the free surface along the centerline of the moonpool are spaced 1m apart to span the length of the moonpool. In most cases the maximum elevations of the free surface are at the first or last field point, adjacent to the ends. A special post-processor is used to search at each frequency for the point of maximum elevation in the moonpool, and then to search for the frequencies where this maximum elevation is again maximized. Convergence tests were performed to achieve an accuracy of 3-4 decimals for the elevations and resonant frequencies. The accuracy of the maximum elevations is less certain very close to the second and third resonant peaks in Figure 3; this may account for the irregular results shown for these modes in Figure 4. The option to remove irregular-frequency effects was used for the calculations of the added-mass coefficients in Figure 5.

The computations of the separate added-mass coefficients in the moonpool and exterior domain, required for the domain-decomposition method, have also been performed with WAMIT. The coefficients A_{ij}^+ for the domain of the moonpool are evaluated using the procedure for internal tanks ([8], Section 12.1). For the approximate procedure in Section 4 the coefficients A_{ij}^- in the exterior domain are evaluated using the zero-frequency option to satisfy the boundary condition $\phi_z^- = 0$ outside the moonpool opening, which is represented by a single patch in the plane $z = 0$. Generalized modes ([8], Chapter 9) are used in both domains to represent the normal velocity on the opening. The computations for the exterior domain in Section 6 use the same generalized-mode procedure, with the barge hull and free-surface effects included in the conventional manner. For the barge with zero draft in Figure 10 the bottom patches are in the plane $z = 0$ and the patches on the ends and sides are removed.

Appendix B – Analytical evaluation of the exterior added mass

With the assumptions stated in Section 4, the exterior domain is bounded above by the plane $z = -d$, which extends to infinity in all directions. The moonpool opening is in this plane, within the rectangle $-a < x < a$, $-w/2 < y < w/2$. The normal velocity on $z = -d$ is specified by (9) in the opening and is equal to zero outside the rectangular boundary. The potential ϕ_i^- can be expressed explicitly in terms of a planar distribution of sources with strength proportional to the normal velocity, and the added-mass coefficients (10) are given by the integrals

$$A_{ij}^- = \frac{1}{2\pi} \int_{-a}^{a} d\xi \int_{-w/2}^{w/2} d\eta \int_{-a}^{a} dx \int_{-w/2}^{w/2} dy \frac{f_i(x) f_j(\xi)}{R}, \tag{31}$$

where

$$R = \sqrt{(x-\xi)^2 + (y-\eta)^2}.$$

If the modal functions f_i are defined by polynomials (31) can be evaluated from integrals of the general form

$$I_{mn} = \int_{-a}^{a} d\xi \int_{-w/2}^{w/2} d\eta \int_{-a}^{a} dx \int_{-w/2}^{w/2} dy \frac{x^m \xi^n}{R}. \tag{32}$$

If $m+n$ is odd $I_{mn} = 0$.

The variables of integration are first changed with the substitutions

$$x - \xi = 2au, \quad x + \xi = 2as, \quad y - \eta = wv, \quad y + \eta = wt.$$

If the integration is performed first with respect to s and t, it follows that

$$I_{mn} = 2a^{m+n+3}\beta^2 \int_{-1}^{1} du \int_{-1}^{1} dv \int_{-1+|u|}^{1-|u|} ds \int_{-1+|v|}^{1-|v|} dt \frac{(s+u)^m (s-u)^n}{\sqrt{u^2 + \beta^2 v^2}}, \tag{33}$$

where $\beta = w/2a$ is the ratio of the width to the length of the opening. The numerator can be expanded using the binomial theorem for arbitrary (m, n). Only even powers of u and s contribute to the integrals.

For the case $(m = n = 0)$

$$\begin{aligned} I_{00} &= 2a^3\beta^2 \int_{-1}^{1} du \int_{-1}^{1} dv \int_{-1+|u|}^{1-|u|} ds \int_{-1+|v|}^{1-|v|} dt (u^2 + \beta^2 v^2)^{-\frac{1}{2}} \\ &= 8a^3\beta^2 \int_{-1}^{1} du (1-|u|) \int_{-1}^{1} dv (1-|v|)(u^2 + \beta^2 v^2)^{-\frac{1}{2}} \\ &= 32a^3\beta^2 \int_{0}^{1} du (1-u) \int_{0}^{1} dv (1-v)(u^2 + \beta^2 v^2)^{-\frac{1}{2}}. \end{aligned} \tag{34}$$

If the remaining variables of integration are changed using the relations

$$u = r\cos\theta, \quad \beta v = r\sin\theta$$

it follows that

$$\begin{aligned} I_{00} &= 32a^3 \left[\int_0^{\theta_1} \int_0^{\sec\theta} + \int_{\theta_1}^{\pi/2} \int_0^{\beta\csc\theta} \right] (1 - r\cos\theta)(\beta - r\sin\theta) dr d\theta \\ &= 32a^3 \left[\int_0^{\theta_1} d\theta (\tfrac{1}{2}\beta\sec\theta - \tfrac{1}{6}\sec^2\theta\sin\theta) + \int_{\theta_1}^{\pi/2} d\theta (\tfrac{1}{2}\beta^2\csc\theta - \tfrac{1}{6}\beta^3\csc^2\theta\cos\theta) \right], \end{aligned} \tag{35}$$

where $\theta_1 = \tan^{-1}(\beta)$. The following integrals are used:

$$\begin{aligned} \int_0^{\theta_1} \sec\theta d\theta &= \log(\tan\theta_1 + \sec\theta_1) = \sinh^{-1}(\beta), \\ \int_{\theta_1}^{\pi/2} \csc\theta d\theta &= \log(\cot\theta_1 + \csc\theta_1) = \sinh^{-1}(1/\beta), \\ \int_0^{\theta_1} \sec^n\theta \sin\theta d\theta &= \frac{\sec^{n-1}\theta_1 - 1}{n-1} = \frac{(1+\beta^2)^{(n-1)/2} - 1}{n-1}, \quad (n > 1), \\ \int_{\theta_1}^{\pi/2} \csc^n\theta \cos\theta d\theta &= \frac{\csc^{n-1}\theta_1 - 1}{n-1} = \frac{(1+1/\beta^2)^{(n-1)/2} - 1}{n-1}, \quad (n > 1). \end{aligned}$$

Thus

$$I_{00}/a^3 = \tfrac{16}{3}(1+\beta^3) - \tfrac{16}{3}(1+\beta^2)^{3/2} + 16\beta^2\sinh^{-1}(1/\beta) + 16\beta\sinh^{-1}(\beta). \tag{36}$$

This result is the same as the integral evaluated by Molin ([5], A.2.1).

Using the same procedure for the case ($m = n = 1$) gives the result

$$\begin{aligned} I_{11}/a^5 &= 2\beta^2 \int_{-1}^{1} du \int_{-1}^{1} dv \int_{-1+|u|}^{1-|u|} ds \int_{-1+|v|}^{1-|v|} dt (u^2+\beta^2 v^2)^{-\frac{1}{2}} (s^2-u^2) \\ &= \tfrac{32}{3}\beta^2 \int_0^1 du(1-3u+2u^3) \int_0^1 dv(1-v)(u^2+\beta^2 v^2)^{-\frac{1}{2}} \\ &= \tfrac{16}{15} \int_0^{\theta_1} \sec^2\theta \sin\theta d\theta + \tfrac{16}{3} \int_{\theta_1}^{\pi/2} \left(\beta^2 \csc\theta - \beta^3 \cos\theta \csc^2\theta + \tfrac{1}{5}\beta^5 \cos^3\theta \csc^4\theta\right) d\theta \\ &= \left(\tfrac{16}{15} - \tfrac{224}{45}\beta^2 - \tfrac{32}{45}\beta^4\right)(1+\beta^2)^{1/2} - \tfrac{16}{15} + \tfrac{16}{3}\beta^3 + \tfrac{32}{45}\beta^5 + \tfrac{16}{3}\beta^2 \sinh^{-1}(1/\beta). \end{aligned} \tag{37}$$

The added-mass coefficients A_{11}^- and A_{22}^- can be evaluated from (36) and (37). The extension of this procedure for other values of (m, n) is straightforward but tedious.

Appendix C – Analytical solution in the moonpool

The moonpool is divided into two domains, separated by the interface ($-a \le x \le a$, $z = -c$). The velocity potentials in each domain are represented by (16-18). Matching of the potentials and normal derivatives is performed on the interface. For this purpose the following integrals are evaluated, with $z = -c$:

$$\int_{-a}^{a} \varphi_i^+ dx = 2a(1-Kc)C_0^{(i)} + \sum_{m=1}^{\infty} C_m^{(i)} I_{m0} Z_m, \tag{38}$$

$$\int_{-a}^{a} \varphi_i^+ \cos k_n(x+a) dx = \sum_{m=1}^{\infty} C_m^{(i)} I_{mn} Z_m, \tag{39}$$

$$\int_{-a}^{a+b} \varphi_{iz}^+ dx = (2a+b)KC_0^{(i)}, \tag{40}$$

$$\int_{-a}^{a+b} \varphi_{iz}^+ \cos\kappa_n(x+a) dx = \left(\frac{2a+b}{2}\right) C_n^{(i)} Z_n'. \tag{41}$$

Here

$$\begin{aligned} I_{mn} = \int_{-a}^{a} \cos\kappa_m(x+a)\cos k_n(x+a) dx &= (-1)^n \frac{\kappa_m \sin 2a\kappa_m}{\kappa_m^2 - k_n^2} \quad (\kappa_m \ne k_n), \\ &= a \qquad\qquad (\kappa_m = k_n,\ m > 0), \end{aligned} \tag{42}$$

and

$$Z_m = 1 - (K/\kappa_m)\tanh\kappa_m c, \tag{43}$$

$$Z_m' = K - \kappa_m \tanh\kappa_m c. \tag{44}$$

In (40) and (41) the boundary condition $\varphi_{iz}^+ = 0$ is used on the bottom of the recess ($a \le x \le a+b$, $z = -c$).

Similarly, from (17) and (18)

$$\int_{-a}^{a} \varphi_1^- dx = 2a\left(c_0^{(1)} - c\right), \tag{45}$$

$$\int_{-a}^{a} \varphi_1^- \cos k_n(x+a)dx \;=\; ac_n^{(1)}, \tag{46}$$

$$\int_{-a}^{a} \varphi_{1z}^- dx \;=\; 2a, \tag{47}$$

$$\int_{-a}^{a} \varphi_{1z}^- \cos \kappa_n(x+a)dx \;=\; I_{n0} + \sum_{m=1}^{\infty} c_m^{(1)} I_{nm} k_m \tanh k_m(d-c), \tag{48}$$

$$\int_{-a}^{a} \varphi_2^- dx \;=\; 2ac_0^{(2)}, \tag{49}$$

$$\int_{-a}^{a} \varphi_2^- \cos k_n(x+a)dx \;=\; a\left(c_n^{(2)} + \frac{d_n^{(2)}}{\cosh k_n(d-c)}\right), \tag{50}$$

$$\int_{-a}^{a} \varphi_{2z}^- dx \;=\; 0, \tag{51}$$

$$\int_{-a}^{a} \varphi_{2z}^- \cos \kappa_n(x+a)dx \;=\; \sum_{m=1}^{\infty} c_m^{(2)} I_{nm} k_m \tanh k_m(d-c). \tag{52}$$

Matching the potentials and normal velocities on the interface is done by equating (38-41) to (45-48) with $i = 1$ and to (49-52) with $i = 2$.

After truncating the series at $m = M$, the following linear system follows for $i = 1$:

$$2a(1-Kc)C_0^{(1)} + \sum_{m=1}^{M} C_m^{(1)} I_{m0} Z_m \;=\; 2a\left(c_0^{(1)} - c\right), \tag{53}$$

$$\sum_{m=1}^{M} C_m^{(1)} I_{mn} Z_m \;=\; ac_n^{(1)}, \tag{54}$$

$$(2a+b)KC_0^{(1)} \;=\; 2a, \tag{55}$$

$$\left(\frac{2a+b}{2}\right) C_n^{(1)} Z_n' \;=\; I_{n0} + \sum_{m=1}^{M} c_m^{(1)} I_{nm} k_m \tanh k_m(d-c). \tag{56}$$

Proceeding in a similar manner for $i = 2$,

$$2a(1-Kc)C_0^{(2)} + \sum_{m=1}^{M} C_m^{(2)} I_{m0} Z_m \;=\; 2ac_0^{(2)}, \tag{57}$$

$$\sum_{m=1}^{M} C_m^{(2)} I_{mn} Z_m \;=\; a\left(c_n^{(2)} + \frac{d_n^{(2)}}{\cosh k_n(d-c)}\right), \tag{58}$$

$$(2a+b)KC_0^{(2)} \;=\; 0, \tag{59}$$

$$\left(\frac{2a+b}{2}\right) C_n^{(2)} Z_n' \;=\; \sum_{m=1}^{M} c_m^{(2)} I_{nm} k_m \tanh k_m(d-c). \tag{60}$$

In these equations the index n takes all values from $n = 1$ to M. If (55-56) are used to eliminate $C_m^{(1)}$ and (59-60) to eliminate $C_m^{(2)}$ the linear system (20) follows, with the order $L = M + 1$.

Appendix D – Added mass of the moonpool at low frequencies

For the domain of the moonpool the added-mass coefficients (10) can be expressed using the divergence theorem as

$$A_{ij}^{+} = \iint_{\mathcal{B}} \phi_i^{+} \phi_{jn}^{+} dS = -\iint_{\mathcal{F}} \phi_i^{+} \phi_{jn}^{+} dS + \iiint_{\mathcal{V}} \nabla \phi_i^{+} \cdot \nabla \phi_j^{+} dV. \tag{61}$$

Here $\mathcal{B}$ and $\mathcal{F}$ are the bottom and free surface of the moonpool and $\mathcal{V}$ is its volume. There is no contribution to the surface integral from the sides or bottom of the recess due to the boundary condition $\phi_{jn}^{+} = 0$. Using the free-surface boundary condition (4) gives

$$A_{ij}^{+} = -\frac{1}{K} \iint_{\mathcal{F}} \phi_{in}^{+} \phi_{jn}^{+} dS + \iiint_{\mathcal{V}} \nabla \phi_i^{+} \cdot \nabla \phi_j^{+} dV, \tag{62}$$

where $K = \omega^2/g$. It is reasonable to assume that $\nabla \phi_i^{+} = \mathrm{O}(1)$ as the frequency tends to zero, and that the free surface is flat with uniform vertical velocity in this limit. Thus from continuity

$$A_{ij}^{+} \simeq -\frac{1}{K} \iint_{\mathcal{F}} \phi_{in}^{+} \phi_{jn}^{+} dS \simeq -\frac{1}{K S_f} Q_i Q_j, \tag{63}$$

where S_f is the area of the free surface and

$$Q_i = \iint_{\mathcal{S}} \phi_{iz}^{+} dS \tag{64}$$

is the volume-flux of fluid across any horizontal plane in the moonpool.

Since $\phi_{1z}^{+} = 1$ on the bottom, Q_1 is equal to the area S_b of the bottom. It follows that

$$A_{11}^{+} \simeq -\frac{S_b^2}{K S_f}. \tag{65}$$

(65) has been derived using slender-body approximations in [9]. The special case of a cylindrical tank is derived from a simple physical argument in [10].

References

[1] X. Guo, H. Lu, J. Yang, T. Peng, Study on hydrodynamic performances of a deep-water drillship and water motions inside its rectangular moonpool, in: Proc. 26th Int Ocean and Polar Engineering Conference, ISOPE, Rhodes, 2016.

[2] X. Guo, H. Lu, J. Yang, T. Peng, Resonant water motions within a recessing type moonpool in a drilling vessel, Ocean Eng. **129** (2017) 228239.

[3] Molin, B. On natural modes in moonpools with recesses, Applied Ocean Research **67** (2017) 1-8.

[4] Faltinsen, O. F. & Timokha, A. N., Sloshing, Cambridge University Press, New York, 2009.

[5] Molin, B., On the piston and sloshing modes in moonpools, J. Fluid Mech. **430** (2001) 27-50.

[6] Newman, J. N., Sortland, B. & Vinje, T. Added mass and damping of rectangular bodies close to the free surface, Journal of Ship Research, **28**, 4, (1984) 219-225.

[7] Fredriksen, A. G., Kristiansen, T. & Faltinsen, O. M., Wave-induced response of a floating two-dimensional body with a moonpool, Phil. Trans. R. Soc. A 373 (2015). http://dx.doi.org/10.1098/rsta.2014.0109

[8] WAMIT, Inc, 'User Manual,' 2016. http://www.wamit.com/manual.htm/.

[9] Newman, J. N., Low-frequency resonance of moonpools, in: Proc. 18th Int. Workshop on Water Waves and Floating Bodies, Le Croisic, France, 2003. http://www.iwwwfb.org/Workshops/18.htm/.

[10] Newman, J. N., 'Wave effects on vessels with internal tanks, in: Proc. 20th Int. Workshop on Water Waves and Floating Bodies, Spitsbergen, Norway, 2005. http://www.iwwwfb.org/Workshops/20.htm/.

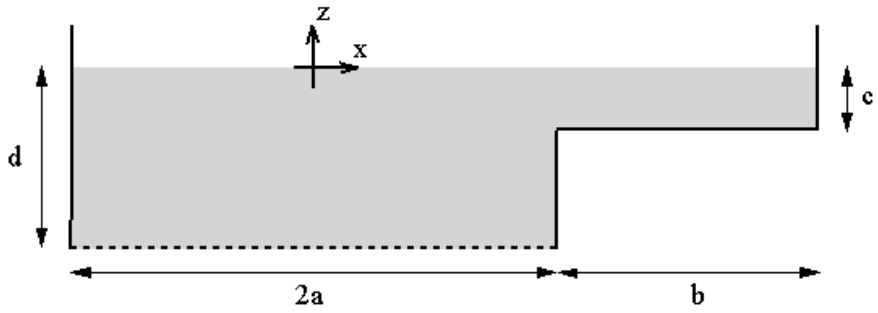

Figure 1: Sketch of the moonpool. The profile shows the base configuration with $a = 14.8$m, $b = 16.0$m, $c = 3.8$m and $d = 11.0$m.

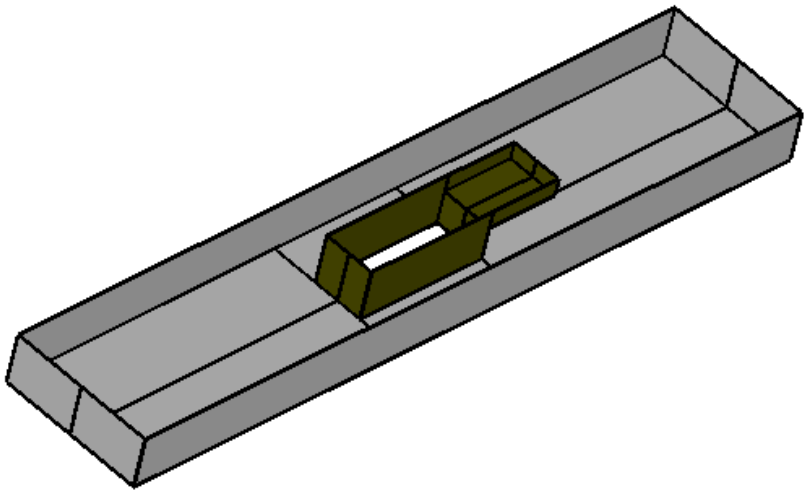

Figure 2: Perspective view of the barge and base moonpool. Only the submerged surface is shown. The principal dimensions of the barge are length=160m, beam=32m, draft=11m. The moonpool width is 11.2m. The other dimensions are shown in Figure 1. The opening below the moonpool is centered at the midship section of the barge.

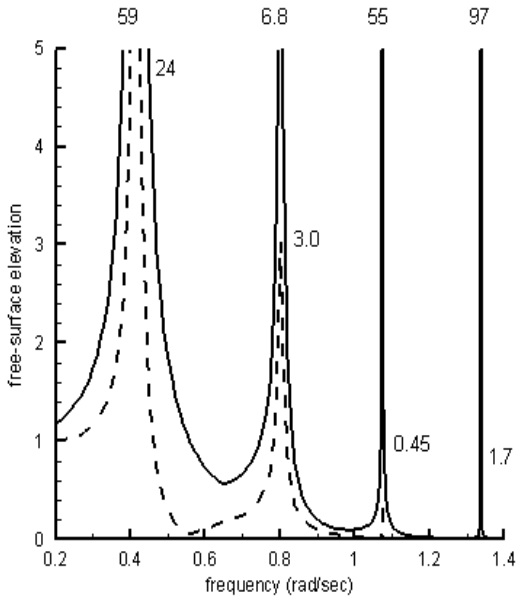

Figure 3: Free-surface elevation in the base moonpool, normalized by the incident-wave amplitude. The solid line is the elevation at the maximum point. The dashed line is the mean value of the elevation over the free surface, equal to the volume-flux divided by the area. The numbers above the peaks indicate their magnitudes at the resonant frequencies. The lower numbers to the right of the peaks indicate the peak values of the mean elevation.

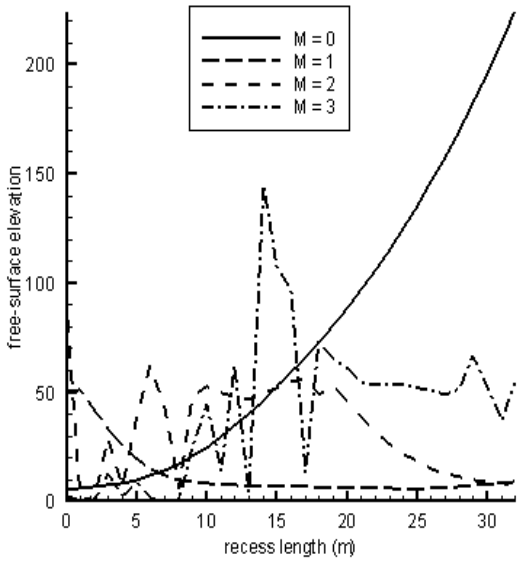

Figure 4: Maximum free-surface elevation in the moonpool at the four resonant frequencies, for varying lengths of the recess. The elevation is normalized by the incident-wave amplitude. $M = 0$ is the piston mode and $M = 1, 2, 3$ are the sloshing modes.

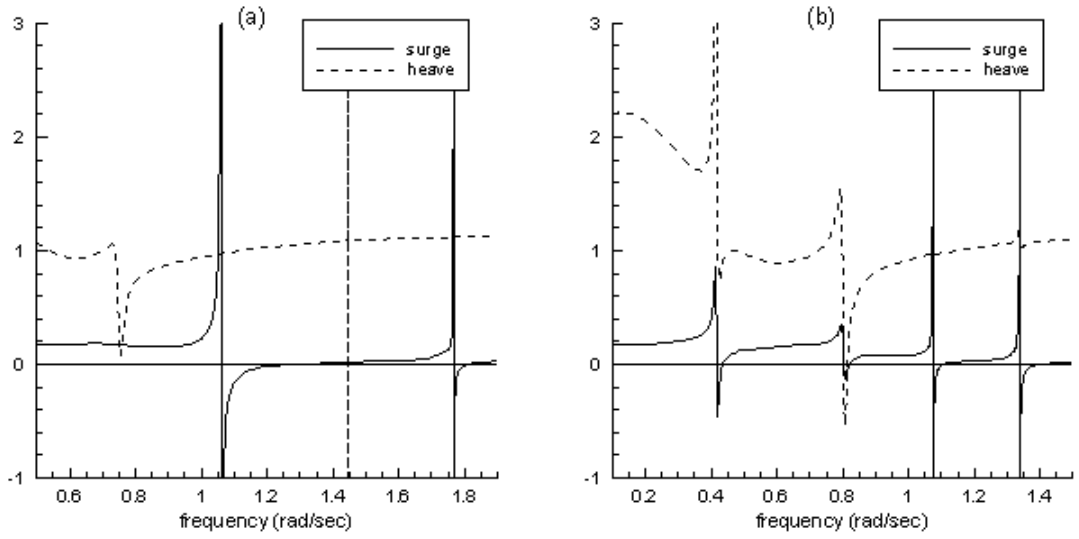

Figure 5: Added-mass coefficients of the barge in the surge and heave modes (a) for the moonpool without a recess and (b) for the base moonpool. The coefficients are normalized by the displaced volume of the barge without the moonpool.

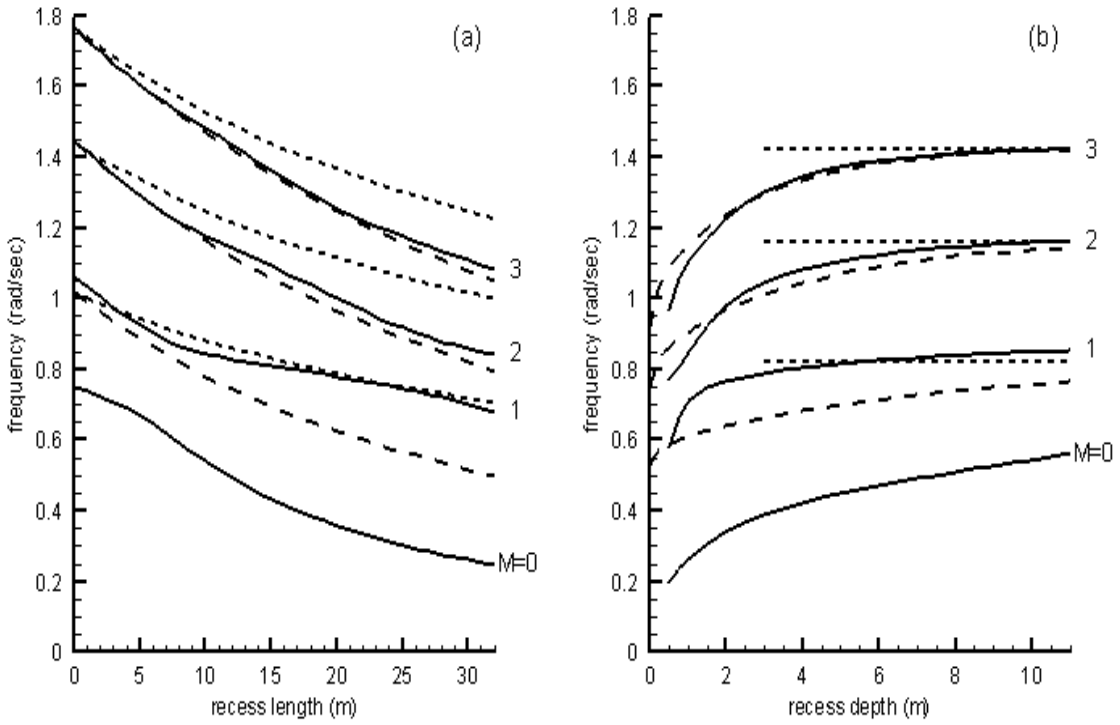

Figure 6: Frequencies of the piston mode (M=0) and first three sloshing modes (M=1,2,3). In (a) the length of the recess is varied from 0 to 32m, with fixed depth 3.8m. In (b) the depth of the recess is varied with fixed length 16m. The solid lines are computed as explained in Section 2, based on the maximum amplitudes of the free-surface elevation in the moonpool. The short dashed lines show the standing-wave frequencies based on the infinite-depth dispersion relation (1). The longer dashed lines show the weighted-average approximation (3).

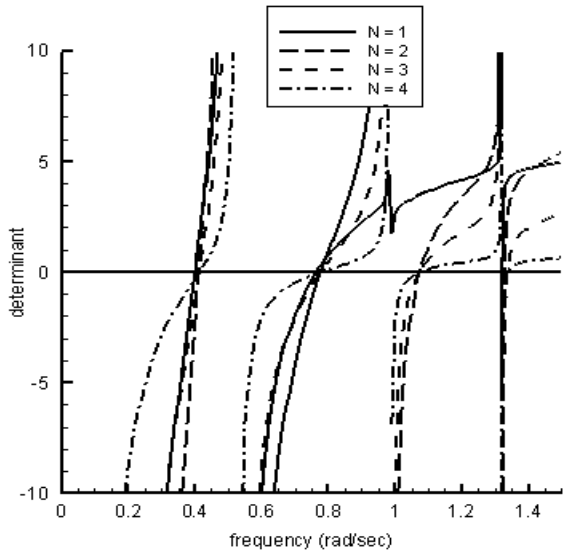

Figure 7: Determinants (13) for the base moonpool configuration with $N = 1, 2, 3, 4$. The values are rescaled, by dividing the added-mass coefficients by 1000. The zero-crossings near $\omega = 0.41, 0.80, 1.07, 1.34$ correspond to the resonant frequencies of the piston mode and first three sloshing modes.

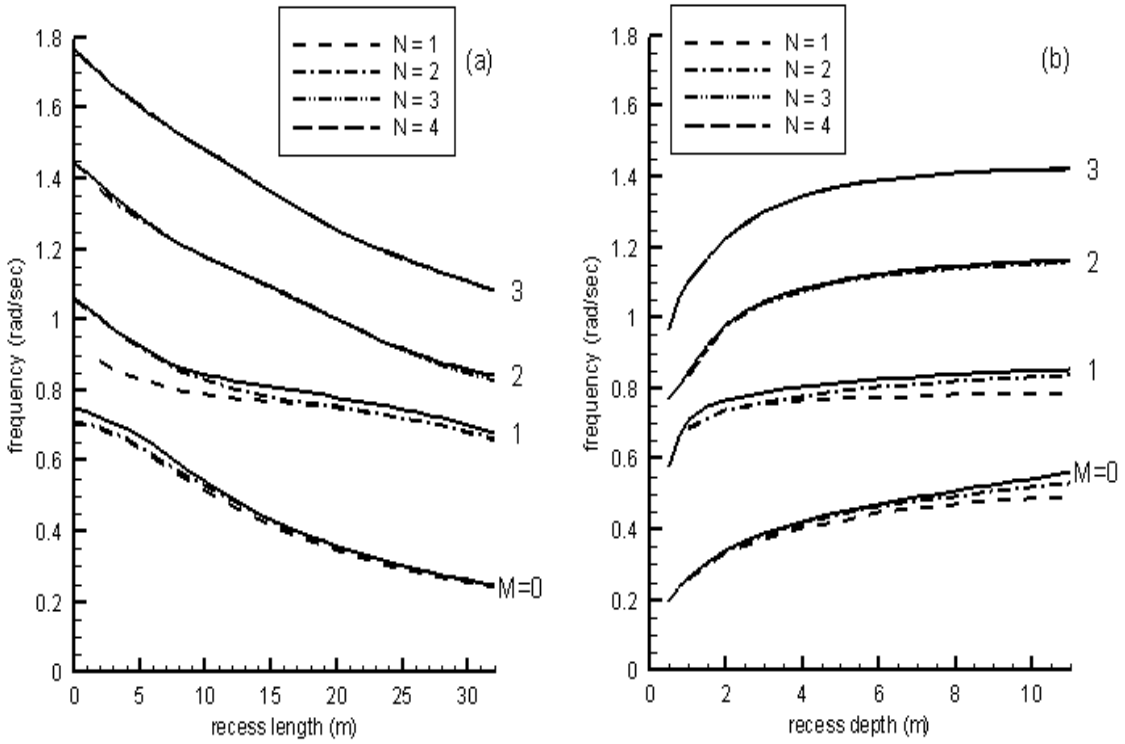

Figure 8: Frequencies of the piston mode ($M = 0$) and first three sloshing modes ($M = 1, 2, 3$), showing the comparison of the results from the analysis in Section 2 (solid lines) with the approximations based on domain decomposition in Section 4. The different broken curves ($N = 1, 2, 3, 4$) are the results based on truncation of the linear system (12) at order N. For the two lowest curves ($M = 0, 1$) only the results for $N = 1, 2$ are plotted; the results for $N = 3, 4$ are identical to $N = 2$ within graphical accuracy. For $M = 2$ the results for $N = 2, 3, 4$ are plotted; these are practically identical except for the recess length equal to zero, where $N = 2$ is not sufficient. Similarly $N = 3$ is not sufficient in this case for $M = 3$, but for all other cases it is practically identical to the result for $N = 4$. For $M = 2, 3$ the approximations are practically identical to the solid lines and cannot be distinguished separately in the plots.

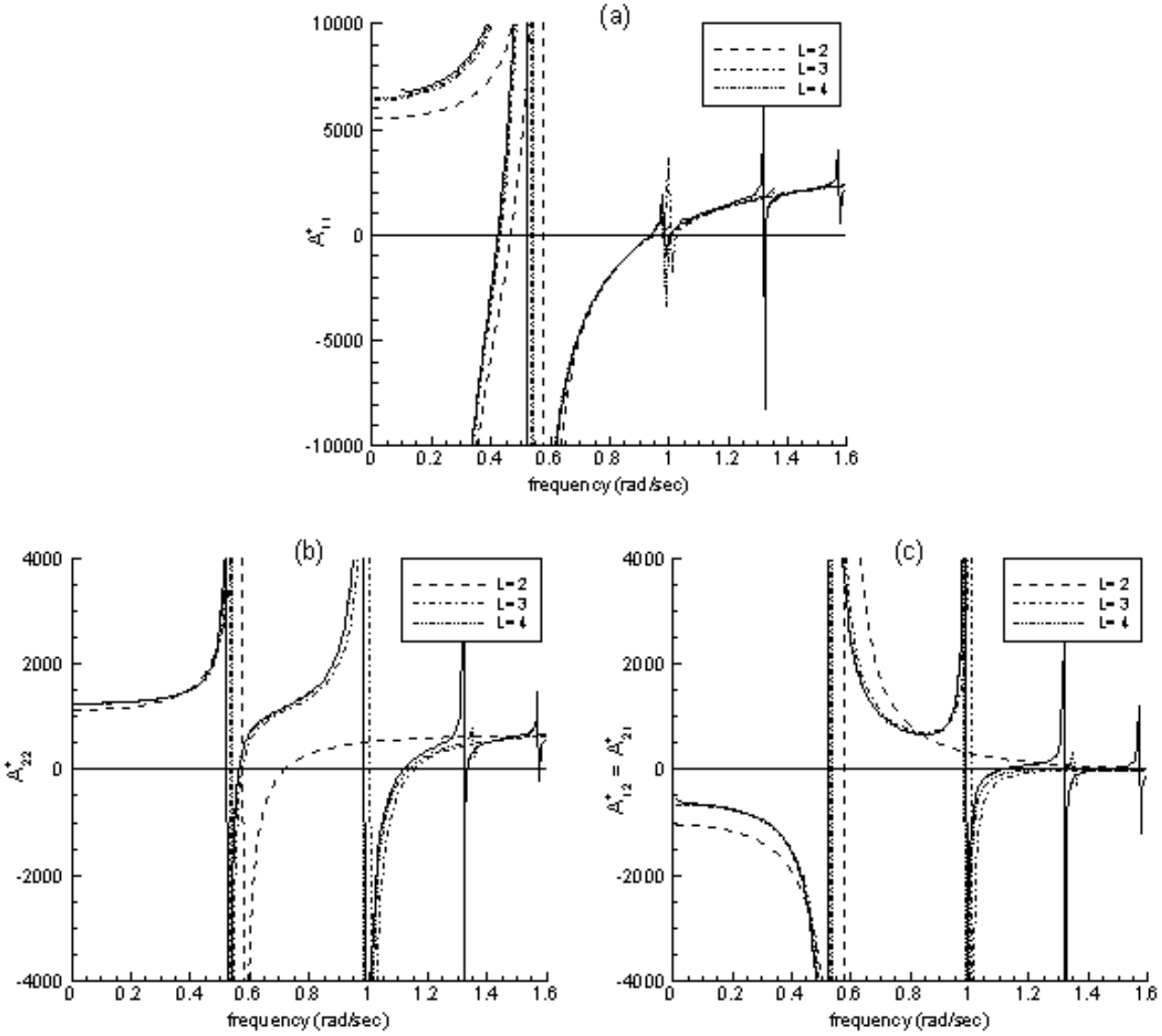

Figure 9: Added-mass coefficients A^+_{11} (a), A^+_{22} (b) and $A^+_{12} = A^+_{21}$ (c) for the base moonpool. The solid lines are computations using WAMIT as described in Appendix A. The broken lines show the results of the analytic method described in Section 5 with the order of the linear systems ($L = 2, 3, 4$). The short curves in the upper left corner of (a) show the modified coefficient $A_{11}+(4a^2w)/K(2a+b)$ with the low-frequency singularity (30) removed. The singularities at $\omega \simeq (0.53,\ 0.99,\ 1.32,\ 1.57)$ are due to the homogeneous solutions associated with the sloshing modes for a closed tank with the same dimensions as the moonpool.

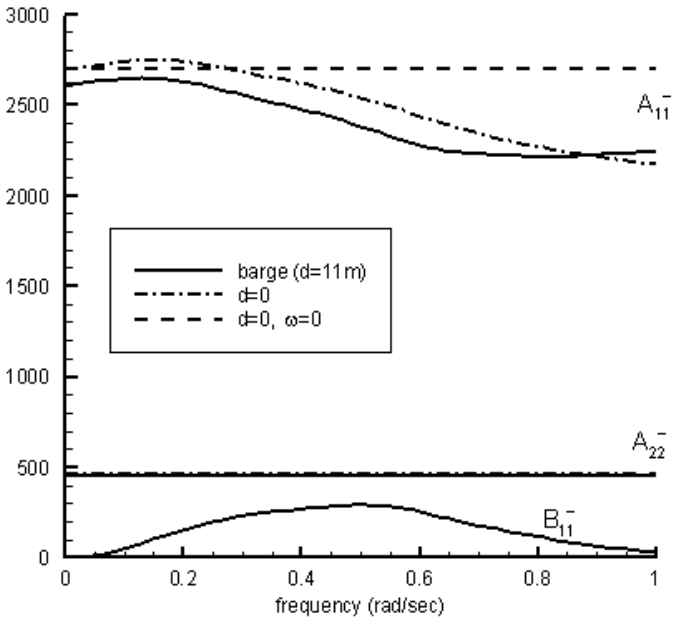

Figure 10: Added-mass coefficients A_{11}^- and A_{22}^- in the external domain, for the heave and pitch modes on the interface at the bottom of the moonpool. The solid lines are evaluated for the barge hull on the free surface, as described in Section 6. The dash-dot curve is for the hull with zero draft, including free-surface effects. The straight dashed lines are for the barge with zero draft and zero frequency, as assumed in the approximations described in Section 4. The lowest curve is the normalized damping coefficient B_{11}^-/ω for mode 1. The damping coefficient B_{22}^-/ω is too small to show in this plot.